BIOMEDICINE

Ultrafast, tough, and adhesive hydrogel based on hybrid photocrosslinking for articular cartilage repair in water-filled arthroscopy

Yujie Hua[1,2†], Huitang Xia[1,3†], Litao Jia[2,3†], Jinzhong Zhao[4], Dandan Zhao[2,3], Xiaoyu Yan[4], Yiqing Zhang[5], Shengjian Tang[3], Guangdong Zhou[1,2,3]*, Linyong Zhu[5,6], Qiuning Lin[6]*

A hydrogel scaffold for direct tissue-engineering application in water-irrigated, arthroscopic cartilage repair, is badly needed. However, such hydrogels must cure quickly under water, bind strongly and permanently to the surrounding tissue, and maintain sufficient mechanical strength to withstand the hydraulic pressure of arthroscopic irrigation (~10 kilopascal). To address these challenges, we report a versatile hybrid photocrosslinkable (HPC) hydrogel fabricated though a combination of photoinitiated radical polymerization and photoinduced imine cross-linking. The ultrafast gelation, high mechanical strength, and strong adhesion to native tissue enable the direct use of these hydrogels in irrigated arthroscopic treatments. We demonstrate, through in vivo articular cartilage defect repair in the weight-bearing regions of swine models, that the HPC hydrogel can serve as an arthroscopic autologous chondrocyte implantation scaffold for long-term cartilage regeneration, integration, and reconstruction of articular function.

INTRODUCTION

Articular cartilage defects with low capacity for self-repair are very common in the clinic; they affect health and mobility and often require surgical intervention for repair (*1*–*3*). Over the past 20 years, tissue-engineering strategies that combine autologous chondrocyte implantation (ACI) with three-dimensional scaffolds have proven effective for generating new cartilage tissue (*4*–*6*). Hydrogels composed by three-dimensional hydrophilic polymer networks are ideal candidate scaffolds for tissue engineering because they can mimic several essential features of the extracellular matrix (ECM) and fit with irregularly shaped defects in situ (*7*–*10*). More recently, in situ gelling strategies based on two-component cross-linking through spontaneous bioconjugate chemistry (*11*–*14*) or enzyme-catalyzed reactions (*15*, *16*) have been developed as injectable hydrogel systems for cartilage tissue repair. Yet, recent findings indicate that photocrosslinking strategies offer better spatiotemporal control and are thus easier to use than two-component cross-linking (*17*–*20*). Wang *et al.* (*21*) showed positive results using an elegant multistep system that applies chondroitin sulfate–based glue for tissue integration followed by photoinitiated radical polymerization hydrogels to promote cartilage regeneration, and a pilot clinical study has even been initiated (*22*). Recently, our group developed an inherent tissue-integration hydrogel using a photoinduced imine cross-linking strategy to embed the exosomes of mesenchymal stem cells to facilitate efficient cartilage regeneration (*23*, *24*).

Despite these achievements, minimally invasive surgical procedures have become increasingly preferred for these repairs in the clinic (*25*, *26*). According to statistics, more than 750,000 arthroscopic meniscal debridement surgeries are performed each year in the United States at an annual cost of about $3 billion, and more than 4 million procedures are performed each year worldwide (*27*). However, the current designs associated with hydrogel-based ACI scaffolds are not suited for arthroscopic approaches. Unlike open surgery, standard arthroscopic procedures require continuous fluid irrigation with a hydraulic pressure of ~10 kPa to expand the lacunar for surgery and adequate visualization (*28*). To accommodate these surgical preferences, the implanted material needs properties that extend beyond the conventional focus of improving biocompatibility for chondrocyte survival and cartilage regeneration. Specifically, arthroscopic surgery requires hydrogels that can gel quickly in water, bind strongly to the surrounding tissue, and maintain mechanical stability to withstand the fluid pressure environment. However, to date, no hydrogel has demonstrated all of these properties simultaneously. In the clinic, gel-like products are blindly injected into the whole joint cavity after evacuating the arthroscopic devices and therefore cannot accurately target the defect site. Alternatively, for targeted application, irrigation must be stopped, and the joint that completely drained of irrigation fluid using a suction cannula and gauze before the hydrogel can be applied (*29*). Therefore, in situ gelling strategies that integrate the properties described above are urgently needed for direct use in fluid-irrigated arthroscopic surgery.

Here, we report a novel and versatile hybrid photocrosslinkable (HPC) method that combines photoinitiated radical polymerization and photoinduced imine cross-linking to fabricate double-network (DN) hydrogels for ACI scaffolds. The introduction of methacrylate-grafted hyaluronic acid (HA) ensures rapid gelation based on free radical–initiated polymerization. After further combination with *o*-nitrobenzyl (NB)–grafted HA (HANB) adhesive, the mechanical performance of the HPC hydrogel was greatly enhanced through DN-associated mechanisms. Simultaneously, the aldehyde groups photogenerated from NB can rapidly react with the amino groups distributed in gelatin (GL) or the surrounding cartilage surfaces.

[1]Department of Plastic and Reconstructive Surgery, Shanghai 9th People's Hospital, Shanghai Key Laboratory of Tissue Engineering, Shanghai Jiao Tong University School of Medicine, Shanghai, China. [2]National Tissue Engineering Center of China, Shanghai, China. [3]Research Institute of Plastic Surgery, Weifang Medical University, Weifang, Shandong, China. [4]Department of Sports Medicine, Shanghai Jiao Tong University Affiliated Sixth People's Hospital, Shanghai, China. [5]Key Laboratory for Advanced Materials and Joint International Research Laboratory of Precision Chemistry and Molecular Engineering, Feringa Nobel Prize Scientist Joint Research Center, School of Chemistry and Molecular Engineering, East China University of Science and Technology, 130# Meilong Road, Shanghai 200237, China. [6]School of Biomedical Engineering, Shanghai Jiao Tong University, Shanghai, China.
*Corresponding author. Email: guangdongzhou@126.com (G.Z.); qiuninglin@sjtu.edu.cn (Q.L.)
†These authors contributed equally to this work.

This reaction results in the formation of high-performance DN hydrogel scaffolds in situ, which synergistically anchor to the surrounding cartilage via imine bonds in one step. The ultrafast gelation, high mechanical strength, and strong adhesion of the HPC hydrogel facilitate its direct use in water-filled arthroscopic surgery in vitro and in vivo. Furthermore, subcutaneous implantation of chondrocyte-loaded HPC hydrogel scaffold in nude mice to regenerate cartilage, in addition to successful healing of articular cartilage defects in the weight-bearing regions of a swine model, together demonstrate that our hybrid photocrosslinking strategy is promising for arthroscopic ACI treatment.

RESULTS

Preparation and characterization of HPC hydrogels

To construct the HPC hydrogel, HANB [molecular weight (M_w) = 340 kDa, 3.5% NB-substituted degree] was first synthesized as described in our previous report (fig. S1) (*23*). HA was chosen because it is an important glycosaminoglycan (GAG) that is found in cartilage (*30*). GL (from porcine skin) was used as the amino precursor of the first network because of its excellent cell adhesion capability (*31*). In addition, methacrylate-modified HA [HAMA; M_w = 48 kDa, 83.1% methacrylate-substituted degree] and a lithium phenyl-2,4,6-trimethylbenzoylphosphinate (LAP) photoinitiator were introduced as the gel precursors of the second network (fig. S2A). The selection of HA M_ws was based on the overall balance of precursor solution viscosity and mechanical performance of the DN hydrogels. The HANB, with higher molecular weight than HAMA, benefits the construction of the sparsely cross-linked and stretchable network necessary for DN hydrogels (*32*); the HAMA, with lower M_w, was selected to avoid excessive viscosity in the gel precursor solution.

The gelation process and mechanical properties of HPC hydrogels with different solid contents [HPC-Low, 9% (w/v), HANB/GL/HAMA = 2:6:1; HPC-High, 17% (w/v), HANB/GL/HAMA = 4:12:1; both with 0.2% (w/v) LAP (6.8 mM)] were compared with two single-network (SN) gels [HANB/GL gel, 8% (w/v), HANB/GL = 2:6; HAMA gel, 1% (w/v) with 0.2% (w/v) LAP] (Fig. 1A and table S1). As shown in Fig. 1 (B and C) and movie S1, the combination of photoinitiated radical polymerization and photoinduced imine cross-linking ensured that the HPC hydrogels gelled rapidly in 1.2 ± 0.2 s through simultaneous photoactivation of the dual cross-linking reactions, whereas the HANB/GL and HAMA gels took 27.9 ± 1.3 s and 4.4 ± 0.3 s to gel, respectively (Fig. 1D and fig. S2B). The final storage moduli (complete gelation) of the HPC hydrogels were markedly greater (6147 ± 231 Pa and 12460 ± 781 Pa for HPC-Low and HPC-High gels, respectively) than those of the HANB/GL (875 ± 39 Pa) and HAMA (1965 ± 42 Pa) gels (Fig. 1E).

The compression stress of the HPC-Low and HPC-High gel was seven- and eightfold greater than that of the HANB/GL gel and 72- and 86-fold greater than that of the HAMA gel (Fig. 1F), respectively. Even when the solid contents of HANB/GL and HAMA gels were supplemented with nonfunctionalized HA to levels equivalent with those in the HPC-Low gel [HANB/GL-Ctrl (control) and HAMA-Ctrl groups in table S1], the mechanical performance was still far below that of the HPC-Low gel. Furthermore, repeated compression tests at strain of 10, 20, and 30% revealed no obvious decline in the mechanical strength of the HPC gels over the compression cycle (Fig. 1, G and H). We thus concluded that the above mechanical performance was attributable to the mechanism of DN enhancement (*32*) in which the rigid and brittle HAMA network helps dissipate mechanical energy under large deformation, while the stretchable HANB/GL network facilitates shape recovery after stress removal. These results showed that the HPC gels had ultrafast gelation rates and high mechanical strength, superior to those of the SN gels.

Adhesion tests of HPC hydrogels

We next performed standard lap shear and burst pressure tests to investigate the tissue-adhesive property of DN gels generated by hybrid photocrosslinking. Lap shear testing based on the ASTM F2255-05 standard was used to determine the shear strength between hydrogel and tissue using two glass slides coated with hog casings as substrate (Fig. 2A). The lap shear strength of the DN hydrogels reached 23.7 ± 1.0 kPa (HPC-Low gel) or 43.1 ± 1.1 kPa (HPC-High gel), which was higher than that of SN hydrogels (3.2 ± 0.3 kPa for the HAMA gel or 11.9 ± 1.2 kPa for the HANB/GL gel). Next, burst pressure testing based on the ASTM F2392-04 standard was performed using hog casings as substrate to test the ability of the adhesive hydrogels to seal tissues under liquid pressure (Fig. 2B). Similar to the results of lap shear strength testing, the burst pressure of DN hydrogels reached 63.4 ± 4.6 kPa (HPC-Low gel) or 78.7 ± 3.1 kPa (HPC-High gel), which were also higher than that of SN hydrogels (10.4 ± 1.4 kPa for the HAMA gel or 32.8 ± 2.8 kPa for the HANB/GL gel). Notably, the enhanced tissue-adhesive capability of the HPC hydrogels rivaled that of fibrin glue, a widely used bioadhesive in the clinic (14.2 ± 1.1 kPa for shear strength and 21.8 ± 2.8 kPa for burst pressure). Together, these results demonstrated that the strength of tissue adhesion is highly related to the performance of hydrogels, and thus DN hydrogels with higher mechanical properties exhibit higher strength of tissue adhesion.

We next examined the adhesion to cartilage by HPC hydrogels using tensile strength and shear tests of the hydrogel-cartilage constructs glued to the plastic sheets. We found that the uniaxial tensile (u) strength and horizontal shear (h) strength (Fig. 2, C and D) of the HPC-Low gel (u = 16.4 ± 1.2 kPa and h = 29.0 ± 3.2 kPa) were markedly greater than those of the HANB/GL (u = 6.8 ± 1.5 kPa and h = 13.1 ± 1.6 kPa) and HAMA (u = 1.3 ± 0.2 kPa and h = 2.6 ± 0.6 kPa) gels (full details in table S2). Furthermore, the tensile and shear forces required to dislocate the HPC gels from the cartilage tissue increased as the hydrogel strength increased (HPC-High gel, u = 33.8 ± 4.6 and h = 47.4 ± 4.9 kPa) [Fig. 2D, correlated with Fig. 1 (E and F)]. However, when the cartilage samples were presoaked in 10% formaldehyde solution to block the amino groups, the binding strength decreased markedly (HPC-Low hydrogel-cartilage constructs, u = 3.5 ± 1.1 kPa and h = 7.2 ± 1.8 kPa; HPC-High hydrogel-cartilage constructs, u = 4.6 ± 2.1 kPa and h = 9.0 ± 2.5 kPa), thereby demonstrating the contribution of chemical anchoring via imine bonds on the hydrogel-cartilage interface. Note that there was a limited decrease in binding strength, regardless of whether photoinduced adhesion occurred in a subaqueous environment or after addition of cells into the gel matrix. The above results indicate that photoinduced imine cross-linking between the HANB adhesive and the cartilage surface results in strong hydrogel-cartilage bonding.

To further scrutinize the integration of HPC hydrogel and cartilage tissue, we used scanning electron microscopy (SEM) to examine the gel-tissue interface. The SEM images revealed a tight and seamless interface between the surrounding cartilage tissue and

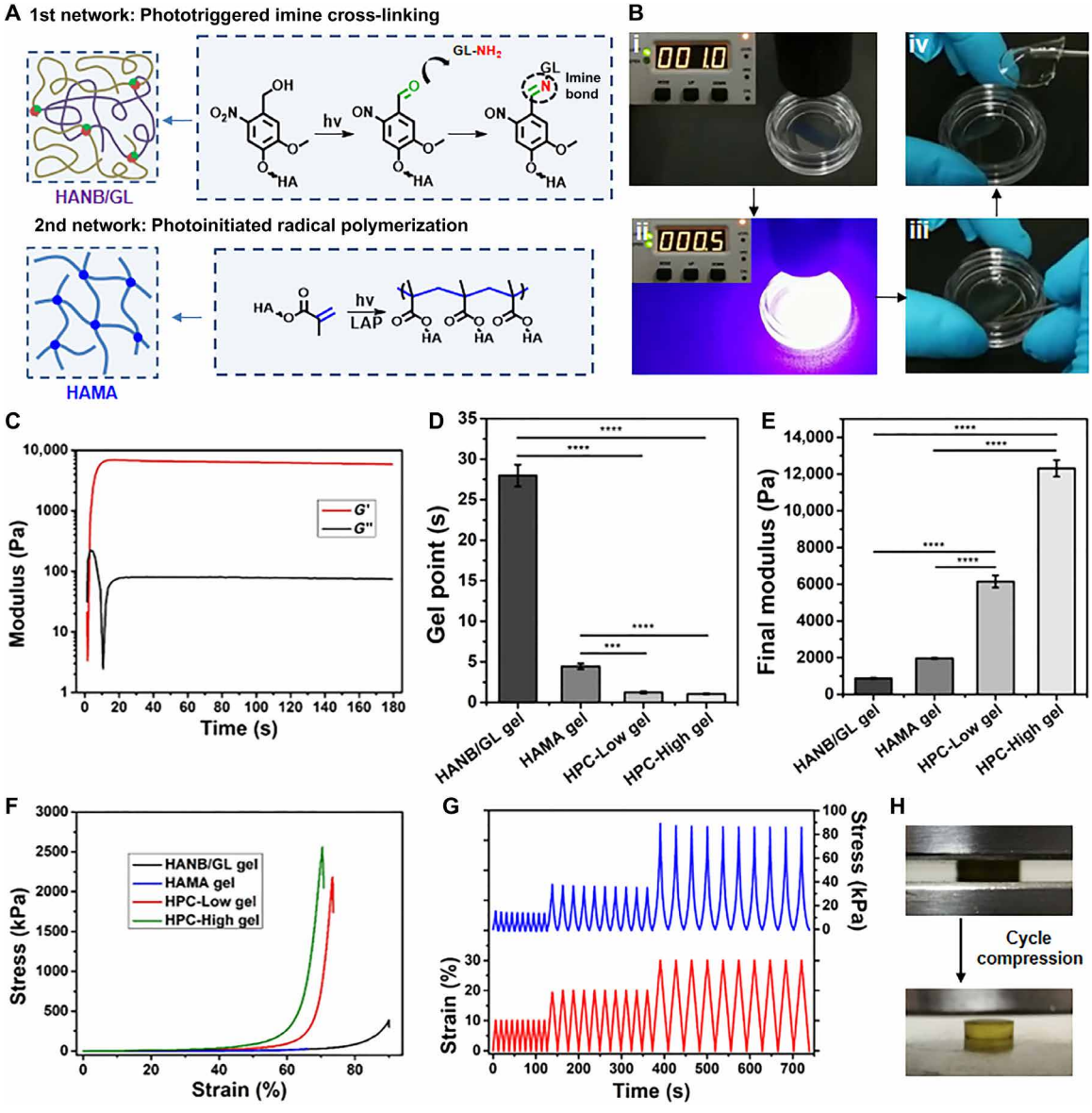

Fig. 1. Rheological and mechanical characterization of HPC hydrogels. (**A**) Schematic illustration of mechanisms for HPC hydrogel construction. (**B**) Photographs showing rapid gelation of the HPC hydrogel within 1 s. (**C**) Representative rheological analysis of the HPC-Low gel. Statistical analysis of (**D**) gel points and (**E**) final storage moduli of the HANB/GL, HAMA, and HPC gels. (**F**) Representative compressive stress-strain curves of the HANB/GL, HAMA, and HPC gels. (**G**) Representative results of repeated compression tests of the HPC-Low gel (10 times at each strain): 10, 20, and 30%. (**H**) Photographs of multiple cycle compressions on HPC-Low gel without any breakage. All the gelling measurements were conducted using a 395-nm light-emitting diode (LED; 50 mW/cm^2). Exposure time, 180 s. $n = 4$; ***$P < 0.001$ and ****$P < 0.0001$. HANB/GL gel, 8% (w/v); HANB/GL = 2:6; HAMA gel, 1% (w/v), 0.2% (w/v) LAP; HPC-Low gel, 9% (w/v); HANB/GL/HAMA = 2:6:1, 0.2% (w/v) LAP; HPC-High gel, 17% (w/v); HANB/GL/HAMA = 4:12:1, 0.2% (w/v) LAP. Photo credit: Yujie Hua, Shanghai Jiao Tong University School of Medicine.

HANB/GL, HPC-Low, and HPC-High hydrogels, respectively (Fig. 3A and fig. S3). In addition, the hydrogels with higher density cross-linkage exhibited tighter network structure and interfacial morphology, consistent with our structural predictions of the hydrogel-cartilage interfaces. By contrast, we observed obvious separation at the interface in the HAMA gel group (fig. S3A), consistent with the non-adhesive property of the HAMA gel.

We then examined the chemical anchor between the HANB adhesive and the cartilage tissue by attenuated total reflection–Fourier transform infrared (ATR-FTIR) spectroscopy and x-ray photoelectron spectroscopy (XPS). To prepare samples coated in a monomolecular layer, a very dilute solution of one-component HANB adhesive [0.1% (w/v)] was used to soak the cartilage samples, instead of the whole hydrogel precursor, followed by 3-min light irradiation. As shown in Fig. 3B, the ATR-FTIR spectrum of the untreated cartilage had typical peaks that were attributable to protein amide-I at 1660 cm^{-1}, to amide-II at 1570 cm^{-1}, and to amide-III at 1260 cm^{-1}. After treatment of the cartilage with HANB adhesive, a characteristic peak attributable to alkoxyl groups appeared at 1020 cm^{-1}, indicating the presence of HA. After irradiation with 395-nm light, new infrared bands appeared at 1705 and 1640 cm^{-1}, which were associated with C═O stretching vibrations and C═N stretching vibrations,

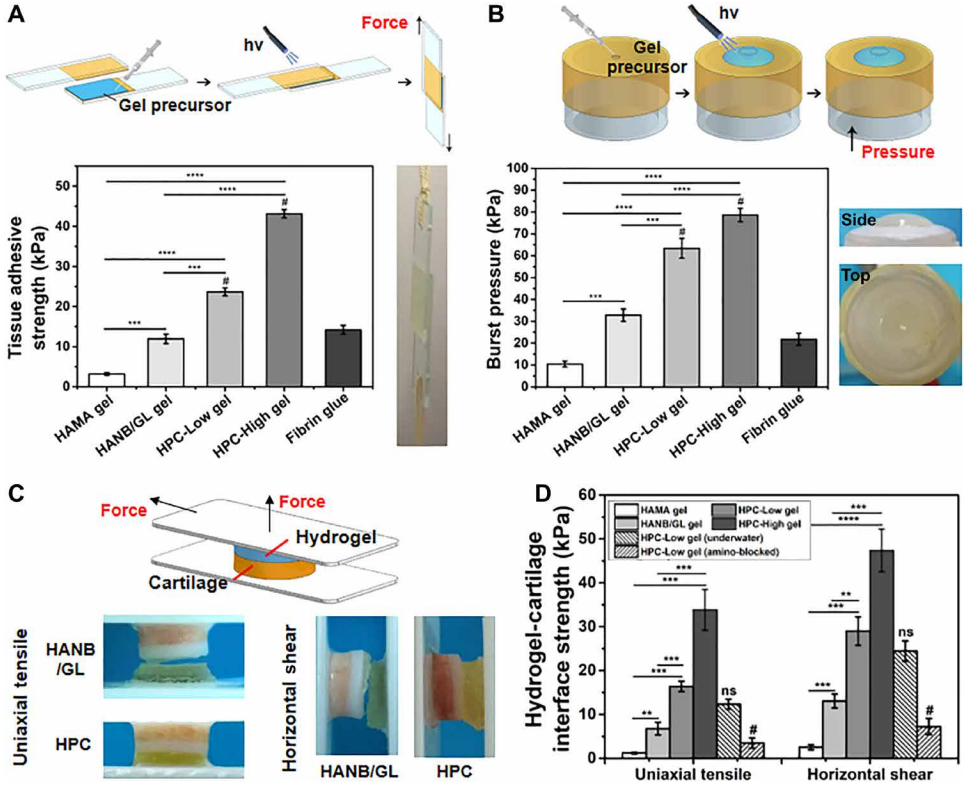

Fig. 2. Adhesion tests of HPC hydrogels. (**A**) Standard lap shear and (**B**) burst pressure tests to determine the hydrogel-tissue binding strength of the HPC hydrogels compared with those of HAMA gel, HANB/GL gel, and Fibrin glue (commercially available sealant). Schematic illustration (top) and photographs (right) of the modified standard methods for lap shear and burst pressure tests. (**C**) Schematic illustration (top) and photographs (bottom) of the uniaxial tensile and horizontal shear tests of the HPC or HANB/GL gel-cartilage interface strength. (**D**) Hydrogel-cartilage interface strength measured by tensile and shear tests. For the amino-blocked group, the cartilage was preprocessed by 10% formaldehyde solution to block the amino groups before use. For the submerged group, the sample of gel-cartilage construct was prepared under water. Light: 395-nm LED, 50 mW/cm^2. Irradiation time, 180 s. $n = 4$; $^{**}P < 0.01$, $^{***}P < 0.001$, $^{****}P < 0.0001$, and $\#P < 0.01$ compared with the HPC-Low gel; ns, no significance. The hydrogel compositions are the same as in Fig. 1. Photo credit: Yujie Hua, Shanghai Jiao Tong University School of Medicine.

respectively. Furthermore, the XPS results revealed that the cartilage treated with HANB adhesive had a larger peak area of C═O (287.8 eV) and C─O (285.8 eV) species than bare cartilage, consistent with the fact that proteoglycan-rich HANB contains more oxygen molecules in both the sugar ring and pendant alcohol groups. After light irradiation treatment, the intensity of the peak attributable to C═O (287.8 eV) increased and a new component associated with C═N bonds appeared at 286.2 eV (Fig. 3C and fig. S2C). This finding confirmed the presence of aldehyde groups photogenerated by HANB and the subsequent formation of imine bonds by photoinduced imine cross-linking on the cartilage surface.

Swelling and biodegradation properties of HPC hydrogels

Swelling and biodegradation are essential properties of hydrogel scaffold–based cartilage tissue engineering. Therefore, we investigated the swelling and biodegradation attributes of HANB/GL, HPC-Low, and HPC-High gels, both in vitro and in vivo (data of HAMA gel are not shown because it was too brittle to implant). The in vitro studies were carried out in Dulbecco's phosphate-buffered saline (D-PBS) with or without hyaluronidase enzyme. The in vivo degradation processes were monitored after subcutaneous implantation in rat models. As shown in table S1, HPC-Low gel showed a low swelling ratio of 108.5 ± 1.9% compared to that of HANB/GL gel (246.9 ± 6.4%). However, as the solid content increased, the swelling ratio of HPC-High hydrogel also increased to 162.8 ± 5.3%. This result is due to a substantially increased capacity for hydration by the doubled solid content of HANB, which overcomes the limited increase in cross-linking density in the first network (gel fraction, 94.8 ± 0.7% for HPC-Low gel and 87.9 ± 1.4% for HPC-High gel), and consequently leads to a higher swelling ratio for the stiffer HPC-High hydrogel. After reaching complete swelling equilibrium, HPC hydrogels stabilized in the buffer solution and underwent enzyme concentration-dependent degradation when supplemented with hyaluronidase (100 or 50 U ml^{-1}) (fig. S4A). Although the stiffer gel exhibited a slower degradation rate, both of materials were completely degraded within 7 days, indicating that HPC gels could be degraded by standard enzymatic mechanisms (*33*).

Further in vivo time-dependent changes in HPC gels were respectively determined by dry weights and volumes of the gel samples at 7, 28, and 56 days after implantation. The results in fig. S4B showed that during the initial swelling period (approximately 7 days), the HPC-High gel showed faster mass loss than HPC-Low gel, which was consistent with calculations of the gel fraction that showed that the addition of excess solid content within the gels led to greater contents of uncross-linked polymer precursors. After attaining swelling equilibrium, the weight of HANB/GL gel decreased sharply because of a rapid rate of degradation, whereas the HPC hydrogels degraded more slowly. In addition, the low swelling ratio and

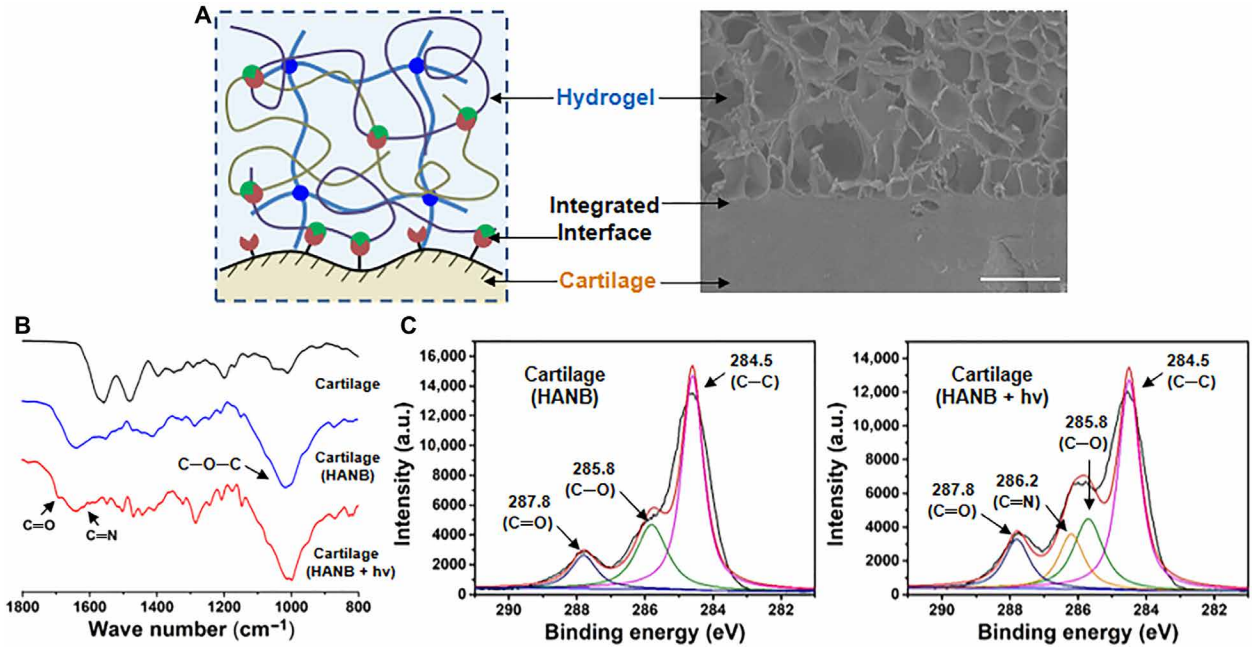

Fig. 3. Integrated interface of the hydrogel-cartilage constructs. (**A**) Schematic illustration of chemical bonding at the interface structure and the corresponding SEM image of HPC hydrogel–cartilage constructs. Scale bar, 500 μm. (**B**) ATR-FTIR spectra and (**C**) C(1s) XPS regions of untreated cartilage and HANB-treated cartilage with or without light irradiation. Light: 395-nm LED, 50 mW/cm^2. Irradiation time, 180 s. The hydrogel compositions are the same as in Fig. 1. a.u., arbitrary unit.

moderate degradation rate for HPC-Low gel compared to that of HANB/GL and HPC-High gels contributed to a low fluctuation in volume, which should benefit the subsequent cartilage repair.

Evaluation of cartilage regenerative capability on different hydrogels

To select the proper hydrogel scaffold for cartilage regeneration, a static subcutaneous implantation model was used for preliminary studies. Briefly, the chondrocyte-loaded hydrogels (HANB/GL, HPC-Low, and HPC-High gels at a density of 100×10^6 cells ml^{-1}) were subcutaneously implanted into nude mice and harvested at 8 weeks to evaluate the maturation degree of generated cartilage. Meanwhile, the hydrogels were intentionally prepared in rosette or star shapes to better evaluate the capability of regenerated cartilage to maintain the shape of the scaffold implants after long-term subcutaneous implantation (Fig. 4, A and B). We found that both HPC-Low and HPC-High groups generally retained their original shapes, while the HANB/GL group lost almost all of its original shape because of insufficient mechanical strength (fig. S5A correlated with Fig. 1F).

Histological examination further confirmed that both HANB/GL and HPC-Low groups displayed better cartilage maturation with homogenous structure, typical lacunae, and cartilage-specific ECM deposition, whereas the HPC-High group presented a hybrid structure with obvious residual material (Fig. 4C and fig. S6). It is possible that the inferior cartilage formation observed in the HPC-High group was due to the stiffness of the network, which limited nutrient diffusion and material degradation (*34*). Further quantification of total collagen, GAG content, and Young's modulus generally agreed with histological results (Fig. 4, D to F). Specifically, the HANB/GL group showed the highest collagen and GAG content and strongest mechanical properties, followed by HPC-Low group, while the HPC-High group exhibited the worst performance. It is worth pointing out that these quantitative results in all groups were lower than those in native samples, potentially because the short in vivo implantation time was insufficient for full material degradation (correlated with fig. S4B) and neomatrix maturation (*35*). In addition, compared with the dynamic environment in normal articular cartilage, the lack of mechanical stimulation in the static environment of the subcutaneous model could also potentially lead to the above differences. In light of its low swelling ratio, appropriate degradation rate, stable shape retention, and effective cartilage regeneration, HPC-Low gel was selected for all the subsequent in vitro and in vivo experiments.

To further demonstrate the importance of sufficient cell density for cartilage regeneration, chondrocyte-loaded HPC-Low gels with different cell densities of 25×10^6, 50×10^6, and 100×10^6 cells ml^{-1} were evaluated by subcutaneous implantation in nude mice. The histological results (fig. S5B) showed that only the 100×10^6 cells ml^{-1} group regenerated homogeneous cartilage, whereas the 25×10^6 and 50×10^6 cells ml^{-1} groups showed obvious heterogeneous structures with hybrid fibrous-like tissue among the regenerated cartilage islands. These results demonstrated that a sufficiently high cell count is required for effective cartilage regeneration when using high-performance DN hydrogel as the scaffold.

Cytocompatibility and biosafety of HPC hydrogels

In consideration of the optimal performance of HPC-Low compared with the other gels, we then evaluated the cytocompatibility of the HPC-Low gel using CCK-8 assays and LIVE/DEAD staining. The gel precursor did not show obvious cytotoxicity (>90% cell viability) for chondrocytes at different concentrations of gel precursor (fig. S7A). Moreover, LIVE/DEAD staining in an in vitro 3D cell culture model revealed that dead cells were largely undetectable at

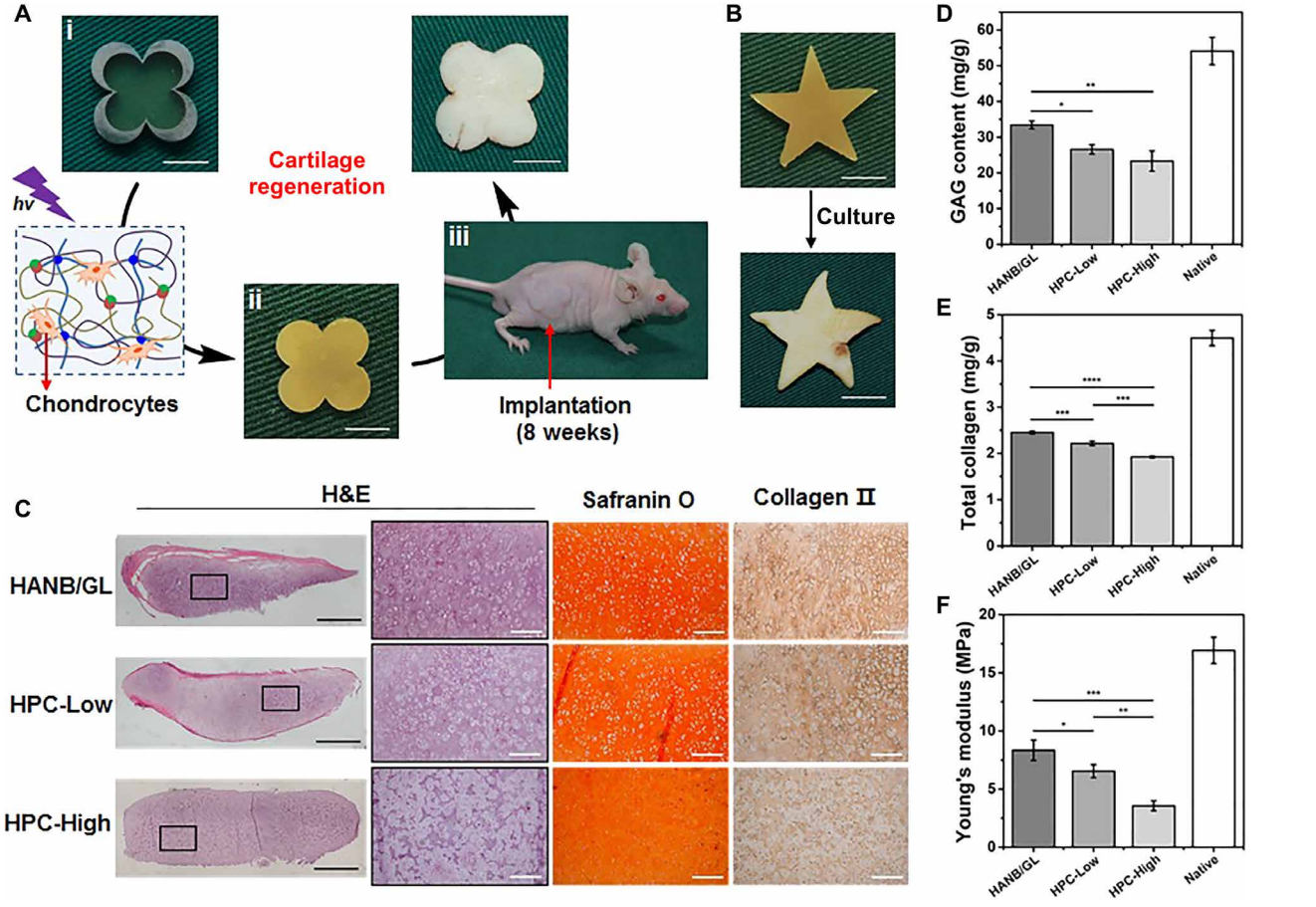

Fig. 4. Tissue-engineered cartilage cultured by subcutaneous implantation in vivo. (**A**) The culture procedures for chondrocyte-loaded HPC-Low hydrogels in rosette or (**B**) star shapes subcutaneously implanted in nude mice. At 8 weeks after the surgery, gross observations show cartilage is ivory white and retains its original shape. Scale bars, 5 mm. (**C**) Representative histological images of H&E, Safranin O, and type II collagen staining of the regenerated cartilage in vivo. Black bars, 1 mm. White bars, 200 μm. (**D** to **F**) Quantitative evaluations of GAG content (D), total collagen (E), and Young's modulus (F) of the regenerated cartilage at 8 weeks after implantation in nude mice ($n = 3$). Light: 395-nm LED, 50 mW/cm^2. Irradiation time, 180 s. The hydrogel compositions are the same as in Fig. 1. *$P < 0.05$, **$P < 0.01$, ***$P < 0.001$, and ****$P < 0.0001$. Photo credit: Huitang Xia, Weifang Medical University.

24 hours after the light-induced encapsulation process, thus demonstrating that the photocrosslinking process exerted no obvious negative effects on cell viability (fig. S7, B and C). No dead cells were detected during the full period of in vitro culture and a slight increase was observed in cell counts over the culture time, indicating stable growth and survival of chondrocytes. All of these above results confirmed the satisfactory cytocompatibility of the HPC-Low hydrogel and its photocrosslinking process.

The biocompatibility and safety of the HPC-Low hydrogel were further evaluated by hematoxylin and eosin (H&E) staining and immunohistochemical staining of macrophages (CD68) and lymphocytes (CD3) at 7 and 28 days after subcutaneous implantation in a rat model (fig. S7D). No obvious tissue adhesion was observed between the hydrogel and its surrounding tissue at either time point. The results of immunohistochemical staining showed that only a thin layer of CD68$^+$ macrophages were observed at the outer edge of the HPC-Low gel at day 7, while these CD68$^+$ cells substantially decreased by day 28. In addition, CD3$^+$ lymphocyte infiltration could not be widely detected at either time point. Notably, the histological structures around the implants had recovered to a thin fibrous feature, similar to that of surrounding native tissue, by day 28. These results indicate that the HPC-Low hydrogel induces only a mild inflammatory response to the host organism.

In vitro feasibility evaluation for HPC hydrogel–based arthroscopic cartilage repair under water

On the basis of the ultrafast gelation, high mechanical strength, and high tissue-adhesion strength, the HPC hydrogel is an appropriate ACI scaffold for subaqueous arthroscopic treatment. To test this possibility, we investigated underwater cartilage repair using the HPC hydrogel. Because arthroscopic surgery requires fluid irrigation, the tools for injection and light irradiation must be convenient and quickly switched to prevent diffusion of the gel precursor from the target site under water. To address this issue, we designed a minimally invasive arthroscopic device with an external diameter of 7 mm that combined a channel with the functions for injection and a fiber optic channel for irradiation within a single tube (Fig. 5A).

The intermediate viscosity of the gel precursor solution (table S1) enabled accurate injection of the HPC-Low gel into the target site (i.e., the cartilage defect), which was submerged in water (Fig. 5B).

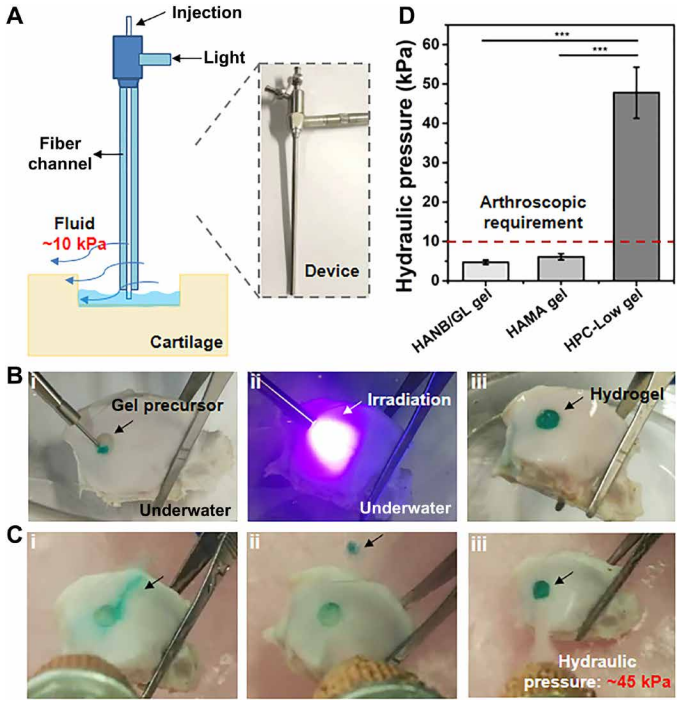

Fig. 5. Feasibility evaluation of HPC hydrogel–based arthroscopic cartilage repair under water in vitro. (**A**) Schematic illustration (left) and photograph (right) of the arthroscopic device with combined hydrogel injection tube and optical fiber channel for curing (7 mm external diameter). (**B**) Photographs of in vitro operation of in situ cartilage defect repair using HPC hydrogel under water: injection of gel precursor (i), light irradiation (ii), and repaired cartilage defect (iii). (**C**) The cured hydrogel-cartilage constructs are flushed with water at various hydraulic pressures: HANB/GL gel (i), HAMA gel (ii), and HPC-Low gel (iii). (**D**) Resistance to water pressure during washing of the repaired cartilage defect by HANB/GL, HAMA, and HPC-Low gels. Fast Green FCF dye is added to the hydrogel for visualization. Light: 395-nm LED, 50 mW/cm^2. Irradiation time, 10 s. $n = 3$, ***$P < 0.001$. The hydrogel compositions are the same as in Fig. 1. Photo credit: Yujie Hua, Shanghai Jiao Tong University School of Medicine.

The gel precursor did not diffuse from the target site within the short time frame needed for irradiation with 395-nm light (approximately 10 s). The hydrogel formation was tightly integrated with the surrounding cartilage tissue and was capable of withstanding a hydraulic pressure of 47.8 ± 6.5 kPa when flushed with water. This pressure is far beyond that typically required by arthroscopic treatment (~10 kPa) (Fig. 5, C and D, and movie S2). However, SN gels were easily washed away, owing to either slow gelation or poor adhesion, and were only able to withstand low hydraulic pressures (2.7 ± 0.6 kPa for the HANB/GL gel and 6.1 ± 0.8 kPa for the HAMA gel).

Evaluation of water-filled arthroscopic ACI treatment based on HPC hydrogel scaffolds in a swine model

On the basis of the results of in vitro tests, we then evaluated the feasibility of arthroscopic cartilage repair using HPC-Low hydrogel in a swine model (Fig. 6A and fig. S8A). The 7-mm-diameter cylindrical, full-thickness, articular cartilage defects, which have been demonstrated to lack the capacity to self-heal (*36*), were created at the weight-bearing regions of the femoral medial and lateral condyles of the knee joint. Arthroscopic treatment of the knee chondral defects was performed under continuous saline irrigation. Saline was supplied from a height of 1.0 m, which resulted in a hydraulic pressure of approximately 10 kPa due to the effects of gravity. As shown in Fig. 6B and movie S3, the HPC-Low gel precursor was injected into the target site and irradiated immediately for 10 s. Consistent with the in vitro experiment, the HPC-Low hydrogel formed rapidly and integrated with the surrounding tissue, even in the saline-filled articular cavity, whereas the SN gels could not be successfully applied under the same conditions. Together, these results indicate that the HPC-Low hydrogels are quick-gelling, mechanically strong, and highly adhesive, even underwater, and are thus well-suited to fluid-irrigated arthroscopic cartilage repair.

To further evaluate the potential of HPC-Low hydrogels in cartilage repair and regeneration when loaded with chondrocytes, we established a swine articular cartilage defect model and closely scrutinized the tissue regeneration process. Autologous ear chondrocytes of passage 2 with specific phenotypes and chondrogenic ability (*37*) were used as the seed cells. The defects were repaired with cell-loaded HPC-Low hydrogel in the experimental (Exp) group or with cell-free HPC-Low hydrogel in the Ctrl group. During the operation, the cell-free and cell-loaded HPC-Low hydrogel precursor solutions both fit well with the defects. They were then gelled in situ and integrated with the surrounding native articular tissue by light irradiation [395-nm light-emitting diode (LED), 50 mW/cm^2]. One of the same pigs was tracked by magnetic resonance imaging (MRI) at different points to monitor the repaired regions. As shown in Fig. 6C and fig. S8B, MRI revealed that both cell-loaded and cell-free HPC-Low hydrogels were effectively retained in the repaired regions. Notably, cartilage regeneration in the Exp group presented a time-dependent trend, which was inferred from the gradual deterioration of the bright water signals (i.e., strong signals shifted to weak signals) (*38*).

After 6 months, the pigs were euthanized to harvest the repaired knee joints for gross observation, histological examinations, and biochemical and biomechanical analyses. From the representative gross view of the repaired regions (Fig. 6D), we found that the defects in the Exp group were well repaired, exhibiting cartilage-like tissue with satisfactory healing at the interfaces. In contrast, incompletely developed cartilage- and fibrosis-like hybrid tissues were observed in the Ctrl group. Histological examination with H&E, Safranin O, and type II collagen staining further confirmed these observations. As shown in Fig. 6E and figs. S9 and S10, the repaired regions in the Exp group exhibited consistent results with relatively homogeneous, hyaline, cartilage-like histological features: mature cartilage lacunae, strong cartilage-specific ECM staining, and a cartilage thickness similar to that of the surrounding normal articular cartilage. Although injury to the calcified layer was unavoidable during defect creation in some animals, as is common and widely reported in previous studies (*39*), and could potentially result in minor aesthetic flaws due to cartilage growth in the subchondral bone (figs. S10, A, B, and D), the newly generated tissues appeared well integrated with the surrounding cartilage and subchondral bone, with good interfacial healing.

By contrast, the control groups showed considerable variability among individuals. Although the repaired regions in the Ctrl groups showed positive staining for GAGs and type II collagen due to the presence of native seed cells, such as the marrow cells derived from bone bleeding during surgery, the repaired regions exhibited obvious tissue disruption, thin cartilage depth, and a rough surface. The

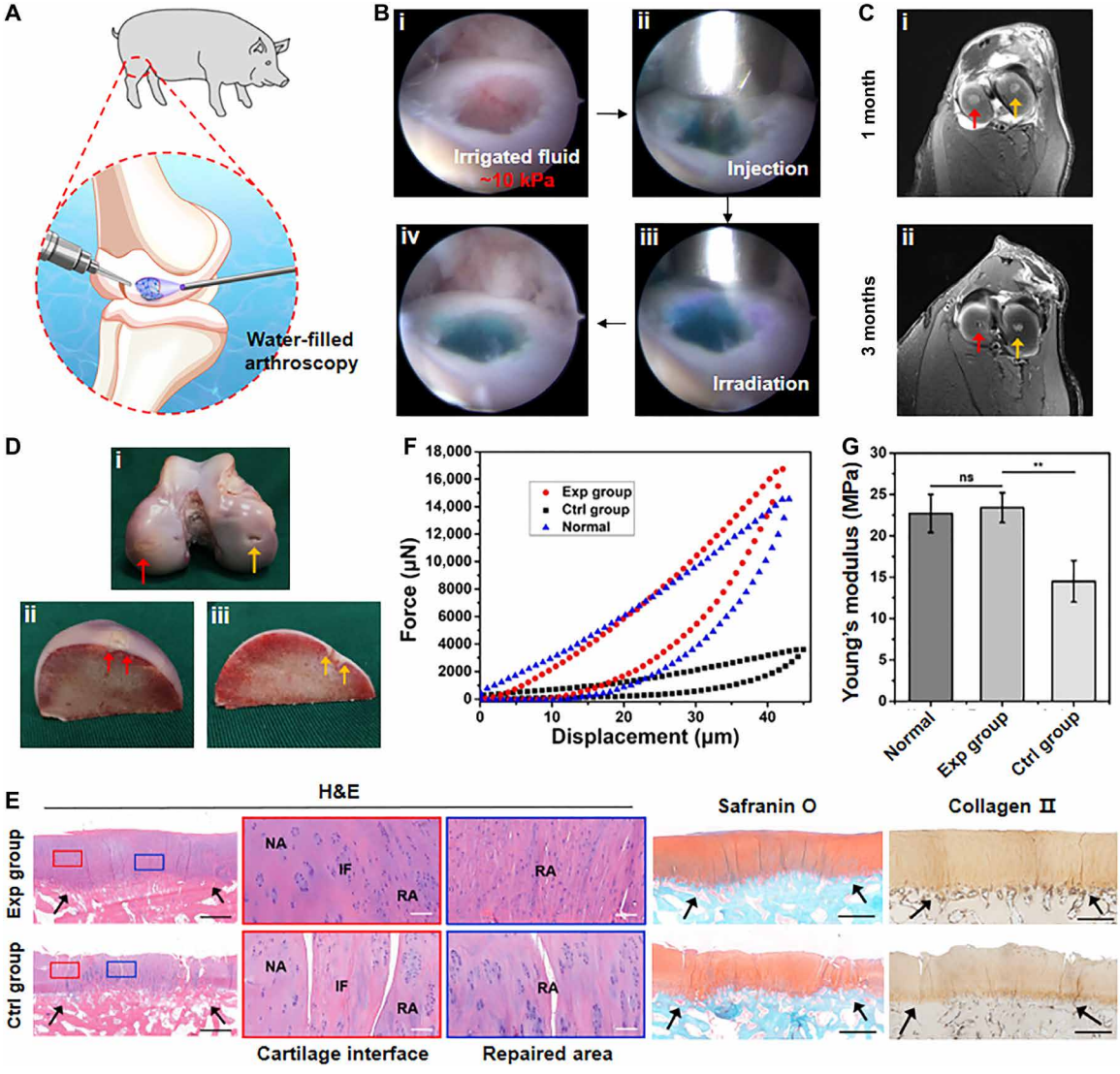

Fig. 6. Evaluation of water-filled arthroscopic ACI treatment based on HPC hydrogel scaffolds in a swine model. (**A**) Schematic illustration of HPC hydrogel application in water-irrigated arthroscopic articular cartilage repair. (**B**) Photographs of in vivo operation of in situ arthroscopic cartilage defect repair using HPC hydrogel under continuous saline irrigation at ~10 kPa: defect (i), injection of gel precursor (ii), light irradiation (iii), and complete repair (iv). Fast Green FCF dye is added to the hydrogel for visualization. (**C**) Representative MRI images (axial) obtained at 1 and 3 months after treatment showing cartilage tissue repair. Exp group, red arrows. Ctrl group, yellow arrows. (**D**) Representative gross view of the repaired regions at 6 months after surgery. Exp group, red arrows. Ctrl group, yellow arrows. (**E**) Representative histological images of H&E, Safranin O, and type II collagen staining of the repaired regions showing strong positive staining of GAGs, ideal interfacial integration with the surrounding native tissues, and satisfactory cartilage regeneration in the Exp group. RA, repaired area; IF, interface; NA, native area. Black arrows indicate repaired regions. Black bars, 1 mm. White bars, 500 μm. (**F**) Representative micromechanical experiment data and (**G**) statistical analysis of Young's moduli of cartilage samples from the repaired regions of the Exp and Ctrl groups and the normal region ($n = 5$). $^{**}P < 0.01$. Photo credit: Huitang Xia, Weifang Medical University.

cartilage defects were so large that cell recruitment based on hydrogel scaffold alone was inadequate to meet the high cell counts required for satisfactory repair of these cartilage defects; thus, unpredictable external factors could remarkably interfere with the repair effects in the control defects, leading to highly inconsistent results. Even in the control animal with the closest histological outcomes to that of the Exp groups, further Sirius red staining indicated that the repaired cartilage in control group was mainly composed of fibrocartilage containing type I collagen rather than hyaline cartilage (fig. S11 correlated with Fig. 6E). Overall, the histological grading scores in the Exp groups were significantly better than those of the Ctrl groups (fig. S12A).

Quantitative analysis of the regenerated cartilage further supported the above observations. The ECM (such as GAGs and total collagen) and DNA contents in the Exp group were significantly higher than those in the Ctrl group, although no significant differences were observed between Exp and Ctrl groups in relative expression levels of chondrogenic marker genes (fig. S12B). As the primary indexes of functionality, compressive strength and Young's modulus in the Exp group reached a comparable level to that of native articular cartilage, significantly higher than those in the Ctrl group (Fig. 6, F and G). Collectively, these results demonstrated satisfactory cartilage regeneration through application of chondrocyte-loaded HPC hydrogel, even in the mechanically demanding weight-bearing regions of the knee joint.

DISCUSSION

The repair of articular cartilage defects is highly challenging clinical procedures. Despite considerable advances in tissue-engineering technology based on hydrogel scaffolds for cartilage repair, hydrogel scaffolds face further challenges for clinical adoption over traditional methods for improving cartilage regeneration due to the general preference for minimally invasive surgery. Different from open surgery, arthroscopic surgical processes that use continuous ~10-kPa fluid irrigation require that hydrogels gel quickly in water, bind strongly to the surrounding tissue, and maintain mechanical stability to withstand the fluid pressure environment and continuous joint movement. However, until now, deficient performance in either operability or mechanical properties—including gelation rate, mechanical strength, and tissue-adhesion ability—have limited in situ gelling techniques in their direct application in arthroscopy surgery.

In the current work, we combine photoinitiated radical polymerization with photoinduced imine cross-linking to develop a novel class of hybrid photocrosslinked hydrogel scaffolds, which exhibit both rapid gelation rates and high tissue-adhesion strength derived from the integration of two different gel networks. The hybrid photocrosslinking strategy accelerates the gelation rate to within 2 s and thus ensures that the highly hydrated gel precursor cures extremely quickly after injection to prevent dilution or diffusion in the pressurized fluid environment. The effective dissipation of mechanical energy by the DN structure increases the mechanical strength of HPC hydrogels (up to ~2 MPa), which, in turn, improves the ability of the hydrogel to adhere to tissue. On the one hand, the chemical anchorage between the photogenerated aldehyde groups of the HANB adhesive and the amino groups distributed on the tissue surfaces results in intrinsically high capacity for tissue adhesion. On the other hand, the strengthened hydrogel-tissue bonding of the HPC hydrogel system can support higher interfacial toughness by dissipating a substantial amount of mechanical energy (*40*, *41*).

To balance the potential restrictions on cartilage regeneration by DN hydrogels with high cross-linking density, a relatively high cell density of 100×10^6 cells ml^{-1} was needed. The HPC hydrogel scaffolds loaded with chondrocytes not only provide appropriate mechanical strength for long-term shape retention but also improve cartilage regeneration, successfully regenerating homogeneous cartilage in static subcutaneous cultures in nude mice. Although static subcutaneous models cannot accurately simulate the dynamic environment of articular cartilage, the results obtained with the subcutaneous model provide direct evidence of a static degradation rate and cartilage regeneration in vivo. Consequently, the HPC hydrogels exhibit ultrafast gelation, appropriate mechanical strength, enhanced tissue adhesion, and homogeneous cartilage regeneration, thus indicating their potential application in arthroscopic cartilage repair.

Another important factor for successful arthroscopic ACI treatment is whether these improved properties are retained in subaqueous applications. Swelling and degradation tests revealed that HPC-Low gel, which has a low solid content, kept its volume more effectively than HPC-High hydrogel, thus ensuring long-term persistence after implantation for accurate cartilage repair. Hence, the HPC-Low hydrogel was selected for the arthroscopic treatment in this work. To accommodate application in minimally invasive surgery, we also designed an arthroscopic device that combines the functions of precursor injection with fiber optic light irradiation. In vitro experiments showed that, after injection, HPC-Low gel precursors quickly cured upon light irradiation and tightly integrated with the surrounding cartilage tissue. Moreover, the cured gels could withstand a hydraulic pressure of 47.8 ± 6.5 kPa, far beyond the ~10 kPa limit required for arthroscopic treatment. Similarly, the HPC-Low hydrogel was relatively easy to apply in the weight-bearing regions of a swine model in vivo, without the need for tedious drying of the irrigation fluid, which is an indispensable step prior to the application of currently used hydrogels. These results thus demonstrated that the superior performance of the HPC-Low hydrogel can be directly applied in minimally invasive surgery in vivo.

Further combination with a sufficient number of chondrocytes resulted in the cell-loaded groups consistently exhibiting more stable and better repair effects than that of cell-free groups. All of the newly generated cartilage in the cell-loaded defects exhibited typical lacunae structures, hyaline cartilage–specific ECM, and tight integration with the surrounding cartilage, and subchondral bone. By comparison with similar previous studies, we found that the current results of cartilage defect repair were essentially consistent with other methods [such as acellular HA hydrogel (*42*), blood clot (*43*), and cell-seeded collagen hydrogel (*44*)]. The acellular hydrogel scaffold can lead to repair of cartilage defects to a limited extent, whereas a cell-loaded hydrogel scaffold can obviously enhance the cartilage repair effects. Unfortunately, because of unavoidable injury of the calcified layer during the creation of cartilage defects, we observed, in some samples, undesirable growth of regenerated cartilage in the subchondral bone, which has also been reported in several previous studies (*39*). To solve this issue, we propose that bone marrow stem cells (BMSCs) may provide a more reliable option than ear-derived chondrocytes for implantation with the HPC hydrogel substrate, since BMSCs have both chondrogenic and osteogenic potential (*45*).

In summary, the current study presents a novel hybrid photocrosslinking strategy for constructing a DN hydrogel as a tissue-engineered ACI scaffold for arthroscopic cartilage repair. The ultrafast gelation, high mechanical strength, and strong adhesiveness of the HPC hydrogel qualify it for direct use in fluid-irrigated arthroscopic surgery. The HPC hydrogel ACI scaffold successfully repaired articular cartilage defects in the weight-bearing regions of a swine model. While this work represents a proof-of-concept study, after refinement and optimization (e.g., to reduce the implanted cell density), we can envision wide adoption of HPC hydrogels as scaffolds in advanced cartilage repair for application in minimally invasive arthroscopic treatments.

MATERIALS AND METHODS

Materials

HA (M_w, 340 or 48 kDa), GL (from porcine skin), methacrylic anhydride, sodium hydroxide, lithium LAP, and 4-(4,6-dimethoxy-1,3,5-triazin-2-yl)-4-methyl morpholinium chloride were purchased from Sigma-Aldrich. All the other chemicals were reagent grade and deionized (DI) water was used.

Synthesis of hydrogel precursors

The synthesis of HANB

HA (2 g, M_w of 340 kDa) was dissolved in 100 ml, 0.1 M 2-morpholinoethanesulfonic acid (MES) solution (pH = 5.17), and 4-(4,6-dimethoxy-1,3,5-triazin-2-yl)-4-methyl morpholinium chloride (0.4 g, 1.36 mmol) was added. NB (60 mg, 0.18 mmol) was dissolved in dimethyl sulfoxide, added into the above solution and

stirred overnight in the dark at 30°C. Then, the solution was dialyzed against DI water for 3 days followed by freezing and lyophilizing. ^{1}H nuclear magnetic resonance (NMR) analysis was performed to determine the substitution degree of the nitrobenzyl group as previously described (*23*).

The synthesis of HAMA

Methacrylic anhydride (8 ml) was added dropwise to a 2% (w/v) HA (2 g, M_w of 48 kDa) solution in an ice bath. The pH was maintained between 8 and 11 adjusted by 5 M NaOH (aq), and the reaction continued overnight in the dark at 4°C. The solution was centrifuged to remove insoluble substance. The pH was adjusted to 7.4 by 1 M HCl (aq). Then, the crude product was dialyzed against DI water for 3 days followed by freezing and lyophilizing. ^{1}H NMR analysis was performed to determine the degree of methacrylation as previously described (*46*). All the other polymers were purchased from Sigma-Aldrich. Hydrogel precursors of HANB, GL, HAMA, and LAP were mixed according to different requirements in D-PBS (pH 7.4) at 37°C. Then, the above specimens were subjected to different measurements following light irradiation (395-nm LED, 50 mW/cm^2).

Rheological analysis

Dynamic rheology experiments were performed on a HAAKE MARS III photorheometer with parallel-plate (P20 TiL, 20 mm diameter) geometry and 395-nm LED (50 mW/cm^2) at 37°C. Time sweep oscillatory tests were performed at a 10% strain [Controlled Deformation (CD) mode], 1-Hz frequency, and a 0.5-mm gap for 180 s. Strain sweeps were performed to verify the linear response. The gel point was determined as the time when the storage modulus (G') surpassed the loss modulus (G''). The final storage modulus, calculated as the balance of rheological tests, was recorded as the final modulus of hydrogels.

Light irradiation time

For all experiments involving the comparison of three groups of materials (HANB/GL gel, HAMA gel, and HPC gel), light irradiation time of 180 s was used for consistency because the control group HANB/GL gel needed 180 s to finish the gelation. For the subsequent animal experiments after abandoning the control group of HANB/GL gel and HAMA gel, a light irradiation time of 10 s was used.

Tests of mechanical properties

Mechanical tests were carried out for as-prepared hydrogels using a GT-TCS-2000 universal material testing machine with 20-kN capacity. For compression tests, hydrogel samples were prepared as cylindrical shapes, 10 mm in diameter and 3 mm long, with speed set at 1 mm/min. The cyclic compression tests were conducted 10 times for each strain at 10, 20, and 30%. The hydrogels were subjected to compression tests after complete gelation upon light irradiation (395-nm LED, 50 mW/cm^2).

Lap shear tests

Lap shear test was performed according to a previous method (*23*). Briefly, a 3.5 × 2.5 cm fresh hog casing was attached to an 8 × 2.5 cm glass slide with cyanoacrylate glue. Then, 100 μl of gel precursor was uniformly dispersed on the surface of the hog casing. A second hog casing was attached to a glass slide and placed on the first glass slide. The obtained test samples were irradiated with a 395-nm LED (50 mW/cm^2) to allow the gel precursor to gel in situ. One side of the sample was fixed, and increasing pull strength was applied to the other side by a GT-TCS-2000 universal material testing machine. Then, the tissue adhesive strength of the hydrogel was calculated according to Eq. 1. Four samples were tested to determine the adhesive strength of each group (n = 4)

$$\text{Tissue adhesive strength} = F/A \quad (1)$$

where F is the pulling stress and A is the adhesive area.

Burst pressure tests

Burst pressure tests were performed according to a previous method (*19*). Briefly, a piece of 4 × 4 cm hog casing was cut and cleaned to remove any excess fat. The hog casing was fixed to the measurement device that was linked to a syringe pump and filled with water. A 2-mm incision was made on the hog casing surface after which the hydrogels were formed in situ on the puncture site. The burst pressure was measured after the complete gelation of the hydrogels. The pressure at which it began to decrease was considered the bursting pressure. Four samples were tested to determine the burst pressure of each group (n = 4).

Measurement of hydrogel-cartilage interface strength

The cartilage samples with a cylindrical shape of 7 mm diameter and 1 mm length were drawn from swine articular cartilage and washed with DI water to clean the surface of cartilage tissue. The hydrogel precursor solution was applied to the cartilage sample, followed by light irradiation (395-nm LED, 50 mW/cm^2) for 3 min. The hydrogel-cartilage samples were glued to plastic sheets for tensile and shear tests. One side of the plastic sheet was fixed, and increasing tensile or shear strength was applied to the other side by adding a certain amount of water to a barrel that was fixed to the glass slide using a string. When the interface was separated, the mass of the water and barrel was recorded. Then, the hydrogel-tissue interface strength was calculated according to Eq. 2. Four samples were tested to determine the hydrogel-tissue interface strength of each group (n = 4)

$$\text{Hydrogel} - \text{cartilage interface strength} = F/A \quad (2)$$

where F is the tensile or shear stress and A is the adhesive area.

SEM analysis of the hydrogel-cartilage interface

To evaluate the integration of the cartilage tissue and hydrogels, the samples were dehydrated by freeze drying immediately. Then, the dehydrated samples were coated with gold-palladium in a Hitachi S-3400N ion sputter and observed.

ATR-FTIR and XPS experiments

The cartilage samples were first washed with DI water to clean the surface of cartilage tissue. Then, 0.1% (w/v) HANB adhesive solution was applied to soak the cartilage sample, followed by light (395-nm LED, 50 mW/cm^2) irradiation for 3 min or without irradiation (control). The treated samples were dried at 40°C for 12 hours. Then, ATR-FTIR spectra were recorded on a Nicolet 6700 FTIR spectrometer. Film characterization using XPS was carried out in an ultrahigh vacuum chamber by an ESCALAB 250Xi XPS system. Then, XPS spectra were analyzed by XPSPEAK software to conduct peak separation.

Swelling property

The cylindrical hydrogel samples (diameter = 10 mm and height = 2 mm) produced according to the above methods were recorded as the initial weight (W_0). For in vitro swelling tests, the hydrogels were fully immersed in PBS solution (pH = 7.4) for complete swelling (24 hours) ($n = 4$). For in vivo time-dependent swelling tests, the as-prepared hydrogels were directly implanted into the subcutaneous tissue of rats ($n = 3$). After implantation for 1, 7, and 14 days, these samples were carefully collected and gently blotted with filter paper to get rid of excess water on their surfaces. When the mass of these hydrogels was constant, the values were recorded as the wet weight (W_t). The swelling ratio was calculated according to the following Eq. 3

$$\text{Swelling ratio} = \frac{W_t}{W_0} \times 100\% \quad (3)$$

Gel fraction tests

The gel fraction (%) is defined as the ratio of the dry gel weight (W_g) to the initial dry weight of the polymer precursor (W_p). For gel fraction tests, the cylindrical hydrogel samples (diameter = 10 mm and height = 2 mm) generated according to the above methods were fully immersed in 10 ml of DI water at 37°C for complete permeation ($n = 4$ for each gel). Every 8 hours, the DI water was refreshed. After 48 hours, the samples were lyophilized and recorded as the dry weight (W_g). The gel fraction (%) was calculated according to the following Eq. 4

$$\text{Gel fraction (\%)} = \frac{W_g}{W_p} \times 100\% \quad (4)$$

Enzyme-mediated degradation tests

For enzyme-mediated degradation tests, the above hydrogels after complete swelling (24 hours) were recorded as the initial weight W_0. Then, hydrogels were incubated in PBS supplemented with or without 100 or 50 U ml^{-1} hyaluronidase (from bovine testes, Sigma-Aldrich) at 37°C ($n = 4$ for each gel). The culture solution was refreshed every day to maintain the enzyme activity. At each time point, these samples were carefully collected, and gently blotted with filter paper to get rid of excess water on the surface. The weight was recorded as W_t. The mass loss (%) was calculated according to the following Eq. 5

$$\text{Mass loss (\%)} = \frac{W_0 - W_t}{W_0} \times 100\% \quad (5)$$

In vivo degradation tests

The cylindrical hydrogel samples (diameter = 10 mm and height = 2 mm) constructed according to the above methods were recorded as the initial wet volume (V_0), then lyophilized, and recorded as the initial dry weight (W_0). The as-prepared hydrogels were directly implanted into the subcutaneous tissue of rats ($n = 3$). After implantation for 7, 28, and 56 days, the hydrogels with the surrounding tissue were harvested after euthanizing rats. These samples were thoroughly washed in distilled water, and the excess tissue was carefully removed. The samples were measured with digital calipers to record the wet volume (V_t), then lyophilized, and recorded as the dry weight (W_t). In vivo degradation and volume change were measured on the basis of the changes in weights and sizes of the samples before and after implantation. The degradation ratio recorded as relative mass (%) and volume change recorded as relative volume % were respectively calculated according to the following equation (Eqs. 6 and 7)

$$\text{Relative mass (\%)} = \frac{W_t}{W_0} \times 100\% \quad (6)$$

$$\text{Relative volume \%} = \frac{V_t}{V_0} \times 100\% \quad (7)$$

Immunohistochemical evaluation by subcutaneous implantation

For immunohistochemical evaluation, HPC-Low hydrogels were subcutaneously implanted into rats. After implantation for 7 and 56 days, the HPC-Low hydrogel samples with surrounding tissue were harvested for immunohistochemical analysis. Then, the samples were fixed with 4% paraformaldehyde, embedded in paraffin, sectioned (5-μm cryosection slides), stained with H&E, and then processed using an immunohistochemical technique as previously reported (*24*). CD3 was detected using rabbit anti-CD3 antibody (1:500; ab16669, Abcam, Cambridge, UK), followed by goat anti-rabbit immunoglobulin G (IgG) H&L [horseradish peroxidase (HRP)] (1:2000; ab205718, Abcam, Cambridge, UK). CD68 was detected using mouse anti-CD68 antibody (1:500; ab31630, Abcam, Cambridge, UK), followed by goat anti-mouse IgG H&L (HRP) (1:2000; ab205719, Abcam, Cambridge, UK).

Cell encapsulation and in vivo implantation

Stainless steel molds were manufactured for in situ gelation according to digital models of two different shapes (rosette and star). Porcine chondrocytes from auricular cartilage were isolated, cultured, and expanded. Briefly, the fresh auricular cartilage was obtained from porcine ear and minced into about 1.0 × 1.0 mm^2 pieces. The cartilage pieces were digested using 0.15 weight % type II collagenase (Worthington Biochemical Corp., Freehold, NJ, USA) to isolate chondrocytes. The cells were harvested, cultured, and expanded in the culture medium [high-glucose Dulbecco's modified Eagle medium (Gibco BRL, Grand Island, NY), 10% fetal bovine serum (Hyclone, Logan, UT, USA), and 1% penicillin/streptomycin/amphotericin B solution] supplemented with basic fibroblast growth factor (5 ng/ml). The P0 chondrocytes were passaged at the ratio of 1:5. The chondrocytes (passage 2) were resuspended in the gel precursor solution for the subsequent preparation of cell-loaded hydrogels. Before using, the cells were stained with type II collagen and Alcian Blue to evaluate cartilage phenotype–specific matrix. Then, the gel precursor solution (HANB/GL, HPC-Low, and HPC-High gels) loaded with different cell densities of chondrocytes (25×10^6, 50×10^6, or 100×10^6 cells ml^{-1}) were poured into the stainless steel molds to fabricate cell-loaded hydrogels with specific shapes upon light irradiation (395-nm LED, 50 mW/cm^2). The cell-loaded hydrogels were then subcutaneously implanted into nude mice. After implantation for 8 weeks, all samples were harvested to evaluate cartilage regeneration.

Histological, biochemical, and biomechanical evaluations of in vivo regenerated cartilage

The above samples were fixed in 4% paraformaldehyde, embedded in paraffin, and sectioned for histological and immunohistochemical analysis. Sections were stained according to previously established

methods with H&E, Safranin O, and type II collagen to evaluate histological structure and cartilage ECM deposition in the regenerated cartilage. Expression of collagen II was detected using rabbit anti-collagen II antibody (1:200; ab34712, Abcam, Cambridge, UK), followed by goat anti-rabbit IgG H&L (HRP) (1:2,000; ab205718, Abcam, Cambridge, UK). The samples were collected and minced to conduct cartilage-related biochemical evaluations for GAG and total collagen quantified by the dimethylmethylene blue assay (DMMB; Sigma-Aldrich), and hydroxyproline assay kit (Sigma-Aldrich), respectively. The quantitative data were analyzed by deducting the background of hydrogel after 8 weeks of culture.

The fresh cartilage-like tissue was prepared as cylindrical shapes, 10 mm in diameter and 2 mm in thickness, using a trepan. Biomechanical tests were conducted with a GT-TCS-2000 universal material testing machine with a 20-kN capacity and with test speed set at 1 mm/min. Young's modulus was determined for each sample and analyzed according to the slope of the stress-strain curve in the linear region to evaluate the mechanical properties of the regenerated cartilage.

The operability of cartilage repair under water using HPC hydrogel in vitro

The cylindrical defect with 7 mm in diameter and 1 mm in length was made on a swine articular cartilage. Then, the gel precursors (HANB/GL, HAMA, and HPC gels) were injected into the target site of the cartilage, which was immersed in water, to fill the defect, followed by immediate light (395-nm LED, 50 mW/cm^2) irradiation for about 10 s to form hydrogels. A hydraulic giant with tunable hydraulic pressure was applied to test the hydrogel-cartilage binding strength. The hydraulic pressure was recorded by a hydraulic pressure gauge (n = 3).

Arthroscopic surgery based on HPC hydrogel in vivo

Knee arthroscopic surgery was performed on a swine model using an arthroscope system (Linvatec T2530 with Cannula/Trocar 100163). An image intensifier (560P High Definition Camera System) with light source (Dyonics 300xl) was used to take photographs. A 30° arthroscope was inserted, and a complete diagnostic evaluation of the knee joint was conducted. Irrigation fluid was then introduced into the joint under continuous saline irrigation with pressure of about 10 kPa by gravity effect of saline with 1.0 m in height. After the approximately 7-mm-diameter cartilage defect was created by an electric driller, debridement was performed with curettes and motorized shavers (ConMed) to completely remove the delaminated cartilage and to obtain a well-defined cartilage defect with a stable margin (injury of the calcified layer accompanied by bone bleeding is uncontrollable during the operation). Then, the gel precursors (HANB/GL, HAMA, and HPC-Low gels) were injected through the hollow channel of the specially designed arthroscopic device into the target site of the cartilage defect. The 395-nm light (50 mW/cm^2) was transmitted through the outer fiber channel for in situ photocrosslinking to form hydrogels. During the injection and irradiation process, it was better to keep the defects horizontal.

Repair of swine articular cartilage defects

A total of five hybrid pigs (6 months old, 40 to 50 kg) were used in this study (Shanghai Jiagan Biological Technology Co., Shanghai, China). Porcine chondrocytes from auricular cartilage were isolated, cultured, and expanded as described above. The chondrocytes (passage 2) were resuspended in the gel precursor solution (100 × 10^6 cells ml^{-1}) for subsequent cell-loaded hydrogels. Then, two cylindrical full-thickness articular cartilage defects (7 mm in diameter, chondral defects) were created at the weight-bearing area of the femoral medial and lateral condyles of the knee joint. Both defects were repaired with cell-loaded HPC hydrogel as the Exp group and with cell-free HPC hydrogel as the Ctrl group. The selection of medial or lateral condyle in Exp and Ctrl groups was random. All animals were allowed to move freely after the operation. The animal care and use committee of Shanghai Jiao Tong University School of Medicine approved all the animal studies for this study.

MRI tracking of cell-free and cell-loaded HPC hydrogels in the repaired regions

To avoid consuming excessive clinical resources and enhancing the risk of animal anesthesia, one of the same pigs was randomly selected for MRI using a 3.0-T MR System (SIGNATM Voyager, GE Medical systems, USA) 1, 3, and 6 months after the operation. All the evaluations were conducted by three blinded experts (X. Lin, L. Lin, and H. Yin) using the magnetic resonance observation of cartilage repair tissue scoring system, with the sagittal T1-FSE (TR, 380 ms; TE, 25.4 ms; matrix, 512 × 512; flip angle, 90°; slice thickness, 3 mm; and spacing between slices, 3.3 mm), sagittal FS-PD (2020/33/512 × 512/90°/3/3.3), sagittal STIR (5000/57.5/512 × 512/90°/3/3.3), coronal STIR (4200/58.9/512 × 512/90°/3/3.3), and axial FS-T2 (2900/59.2/512 × 512/90°/4/4.5) sequences as previously described (*38*).

Gross observation and histological examination of repaired regions

Six months after the operation, all the pigs were euthanized to harvest repaired knee joints (distal part of femur). Harvested tissues were sawed sagittally at the midline of repaired regions for gross observation, histological examination, and histological grading scores. All the samples were fixed in 4% paraformaldehyde, embedded in paraffin, and sectioned for histological analysis. Sections were stained according to previously established methods with H&E, Safranin O, and type II collagen to evaluate histological structure and cartilage ECM deposition in the repaired regions. Specially, Sirius red staining was used to distinguish the type of collagen in the repaired regions. Observations were performed with a Nikon LV-UEPI model microscope using crossed polarizing filters. Expression of collagen II was detected using rabbit anti-collagen II antibody (1:200; ab34712, Abcam, Cambridge, UK), followed by goat anti-rabbit IgG H&L (HRP) (1:2000; ab205718, Abcam, Cambridge, UK). The histological grading scores for cartilage repair were performed on the basis of previously reported methods (*47*).

Biomechanical and biochemical evaluations of cartilage tissue

The fresh articular cartilage samples were directly subjected to biomechanical tests. Then, the micromechanical properties were tested using a FT-MTA02 nanoindentor, and the cartilage samples were subjected to a cycle of loading and unloading with 45-μm pressed depth. The size of the silicon probe was 50 × 50 μm, and the speed was set at 100 μm/min. The stiffness of cartilage tissue was determined as the slope of the unloading curve at the site of 90%. Then, the Young's modulus of the cartilage tissue was calculated according to Eq. 8. Five samples were tested to determine the Young's modulus of each group (n = 5)

$$E = \frac{\sqrt{\pi}}{2} \bullet \frac{S}{\sqrt{A}} \quad (8)$$

where E is the Young's modulus, S is the stiffness, and A is the area of indentation.

For biochemical evaluations, the same surgeries of articular cartilage repair on another three hybrid pigs (6 months old, 40 to 50 kg) were performed according to the above methods (Shanghai Jiagan Biological Technology Co., Shanghai, China). Three months after the operation, all the pigs were euthanized to harvest repaired knee joints (distal part of femur). The samples were collected and minced to conduct cartilage-related biochemical evaluations ($n = 3$) for GAG, total collagen, and DNA quantifications, which were quantified by the DMMB (Sigma-Aldrich), hydroxyproline assay kit (Sigma-Aldrich), and PicoGreen dsDNA assay (Invitrogen). The expression levels of chondrogenesis marker (COL1A1, COL2A1, and SOX9) were analyzed by quantitative real-time polymerase chain reaction using an ABI ViiA7 RT-PCR system (Applied Biosystems). The relative expressions were determined by normalizing expression of each C_t value to β-actin C_t value. Three replicate tests were conducted for each sample in the biochemical evaluation process, and the average value was calculated for data analysis.

Statements

All animal experimental procedures were approved by the Independent Ethics Committee of Shanghai Ninth People's Hospital, Shanghai Jiao Tong University School of Medicine. All experiments were conducted in accordance with guidelines from the Division of Laboratory Animal Medicine. All images in Fig. 6 (and figs. S9 and S10) show representative, typical, and reproducible responses to treatment.

Statistical analysis

All data were presented as means ± SD. Differences between the values were evaluated using one-way analysis of variance (ANOVA) with $P < 0.05$ considered statistically significant.

SUPPLEMENTARY MATERIALS

Supplementary material for this article is available at http://advances.sciencemag.org/cgi/content/full/7/35/eabg0628/DC1

View/request a protocol for this paper from *Bio-protocol*.

REFERENCES AND NOTES

1. D. J. Huey, J. C. Hu, K. A. Athanasiou, Unlike bone, cartilage regeneration remains elusive. *Science* **338**, 917–921 (2012).
2. J. Klein, Repair or replacement – A joint perspective. *Science* **323**, 47–48 (2009).
3. E. A. Makris, A. H. Gomoll, K. N. Malizos, J. C. Hu, K. A. Athanasiou, Repair and tissue engineering techniques for articular cartilage. *Nat. Rev. Rheumatol.* **11**, 21–34 (2015).
4. Y. Li, Y. Xiao, C. Liu, The horizon of materiobiology: A perspective on material-guided cell behaviors and tissue engineering. *Chem. Rev.* **117**, 4376–4421 (2017).
5. M. Brittberg, Autologous chondrocyte implantation—Technique and long-term follow-up. *Injury* **39**, 40–49 (2008).
6. S. Marlovits, P. Zeller, P. Singer, C. Resinger, V. Vecsei, Cartilage repair: Generations of autologous chondrocyte transplantation. *Eur. J. Radiol.* **57**, 24–31 (2006).
7. Y. S. Zhang, A. Khademhosseini, Advances in engineering hydrogels. *Science* **356**, eaaf3627 (2017).
8. J. Thiele, Y. Ma, S. M. C. Bruekers, S. Ma, W. T. S. Huck, 25th Anniversary article: Designer hydrogels for cell cultures: A materials selection guide. *Adv. Mater.* **26**, 125–148 (2014).
9. K. Hayashi, F. Okamoto, S. Hoshi, T. Katashima, D. C. Zujur, X. Li, M. Shibayama, E. P. Gilbert, U. Chung, S. Ohba, T. Oshika, T. Sakai, Fast-forming hydrogel with ultralow polymeric content as an artificial vitreous body. *Nat. Biomed. Eng.* **1**, 0044–0051 (2017).
10. E. S. Sani, A. Kheirkhah, D. Rana, Z. Sun, W. Foulsham, A. Sheikhi, A. Khademhosseini, R. Dana, N. Annabi, Sutureless repair of corneal injuries using naturally derived bioadhesive hydrogels. *Sci. Adv.* **5**, eaav1281 (2019).
11. B. Balakrishnan, R. Banerjee, Biopolymer-based hydrogels for cartilage tissue engineering. *Chem. Rev.* **111**, 4453–4474 (2011).
12. C. A. Vilela, C. Correia, J. M. Oliveira, R. A. Sousa, J. Espregueira-Mendes, R. L. Reis, Cartilage repair using hydrogels: A critical review of in vivo experimental designs. *ACS Biomater Sci. Eng.* **1**, 726–739 (2015).
13. L. Cao, B. Cao, C. Lu, G. Wang, L. Yu, J. Ding, An injectable hydrogel formed by in situ cross-linking of glycol chitosan and multi-benzaldehyde functionalized PEG analogues for cartilage tissue engineering. *J. Mater. Chem. B* **3**, 1268–1280 (2015).
14. R. Jin, L. S. M. Teixeira, A. Krouwels, P. J. Dijkstra, C. A. Blitterswijk, M. Karperien, J. Feijen, Synthesis and characterization of hyaluronic acid–poly(ethylene glycol) hydrogels via Michael addition: An injectable biomaterial for cartilage repair. *Acta Biomater.* **6**, 1968–1977 (2010).
15. G. M. Peretti, J.-W. Xu, L. J. Bonassar, C. H. Kirchhoff, M. J. Yaremchuk, M. A. Randolph, Review of injectable cartilage engineering using fibrin gel in mice and swine models. *Tissue Eng.* **12**, 1151–1168 (2006).
16. L. S. M. Teixeira, S. Bijl, V. V. Pully, C. Otto, R. Jin, J. Feijen, C. A. Blitterswijk, P. J. Dijkstra, M. Karperien, Self-attaching and cell-attracting in-situ forming dextran-tyramine conjugates hydrogels for arthroscopic cartilage repair. *Biomaterials* **33**, 3164–3174 (2012).
17. T. E. Brown, K. S. Anseth, Spatiotemporal hydrogel biomaterials for regenerative medicine. *Chem. Soc. Rev.* **46**, 6532–6552 (2017).
18. E. R. Ruskowitz, C. A. DeForest, Photoresponsive biomaterials for targeted drug delivery and 4D cell culture. *Nat. Rev. Mater.* **3**, 17087–17104 (2018).
19. N. Annabi, Y.-N. Zhang, A. Assmann, E. S. Sani, G. Cheng, A. D. Lassaletta, A. Vegh, B. Dehghani, G. U. Ruiz-Esparza, X. Wang, S. Gangadharan, A. S. Weiss, A. Khademhosseini, Engineering a highly elastic human protein–based sealant for surgical applications. *Sci. Transl. Med.* **9**, eaai7466 (2017).
20. Z. Liu, Q. Lin, Y. Sun, T. Liu, C. Bao, F. Li, L. Zhu, Spatiotemporally controllable and cytocompatible approach builds 3D cell culture matrix by photo-uncaged-thiol Michael addition reaction. *Adv. Mater.* **26**, 3912–3917 (2014).
21. D.-A. Wang, S. Varghese, B. Sharma, I. Strehin, S. Fermanian, J. Gorham, D. H. Fairbrother, B. Cascio, J. H. Elisseeff, Multifunctional chondroitin sulphate for cartilage tissue-biomaterial integration. *Nat. Mater.* **6**, 385–392 (2007).
22. B. Sharma, S. Fermanian, M. Gibson, S. Unterman, D. A. Herzka, B. Cascio, J. Coburn, A. Y. Hui, N. Marcus, G. E. Gold, J. H. Elisseeff, Human cartilage repair with a photoreactive adhesive-hydrogel composite. *Sci. Transl. Med.* **5**, 167ra6 (2013).
23. Y. Yang, J. Zhang, Z. Liu, Q. Lin, X. Liu, C. Bao, Y. Wang, L. Zhu, Tissue-integratable and biocompatible photogelation by the imine crosslinking reaction. *Adv. Mater.* **28**, 2724–2730 (2016).
24. X. Liu, Y. Yang, Y. Li, X. Niu, B. Zhao, Y. Wang, C. Bao, Z. Xie, Q. Lin, L. Zhu, Integration of stem cell-derived exosomes with in situ hydrogel glue as a promising tissue patch for articular cartilage regeneration. *Nanoscale* **9**, 4430–4438 (2017).
25. A. Kirkley, T. B. Birmingham, R. B. Litchfield, J. R. Giffin, K. R. Willits, C. J. Wong, B. G. Feagan, A. Donner, S. H. Griffin, L. M. D'Ascanio, J. E. Pope, P. J. Fowler, A randomized trial of arthroscopic surgery for osteoarthritis of the knee. *N. Engl. J. Med.* **359**, 1097–1107 (2008).
26. M. Ochi, N. Adachi, H. Nobuto, S. Yanada, Y. Ito, M. Agung, Articular cartilage repair using tissue engineering technique-novel approach with minimally invasive procedure. *Artif. Organs* **28**, 28–32 (2004).
27. R. A. C. Siemieniuk, I. A. Harris, T. Agoritsas, R. W. Poolman, R. Brignardello-Petersen, S. V. Velde, R. Buchbinder, M. Englund, L. Lytvyn, C. Quinlan, L. Helsingen, G. Knutsen, N. R. Olsen, H. Macdonald, L. Hailey, H. M. Wilson, A. Lydiatt, A. Kristiansen, Arthroscopic surgery for degenerative knee arthritis and meniscal tears: A clinical practice guideline. *BMJ* **357**, j1982 (2017).
28. M. Tey, J. Mas, X. Pelfort, J. C. Monllau, Arthroscopic treatment of hip chondral defects with bone marrow stimulation and BST-CarGel. *Arthrosc. Tech.* **4**, e29–e33 (2015).
29. M. F. Tahoun, M. Tey, J. Mas, T. A. Eid, J. C. Monllau, Arthroscopic repair of acetabular cartilage lesions by chitosan-based scaffold: Clinical evaluation at minimum 2 years follow-up. *Arthroscopy* **34**, 2821–2828 (2018).
30. J. A. Burdick, G. D. Prestwish, Hyaluronic acid hydrogels for biomedical applications. *Adv. Mater.* **23**, H41–H56 (2011).
31. X. Z. Shu, Y. Liu, F. Palumbo, G. D. Prestwich, Disulfide-crosslinked hyaluronan-gelatin hydrogel films: A covalent mimic of the extracellular matrix for in vitro cell growth. *Biomaterials* **24**, 3825–3834 (2003).
32. J. P. Gong, Materials both tough and soft. *Science* **344**, 161–162 (2014).
33. H. G. Garg, C. A. Hales, Biodegradation of Hyaluronan, in *Chemistry and Biology of Hyaluronan* (Elsevier, London, ed. 1, 2004), pp. 71–83.
34. H. Lee, L. Gu, D. J. Mooney, M. E. Levenston, O. Chaudhuri, Mechanical confinement regulates cartilage matrix formation by chondrocytes. *Nat. Mater.* **16**, 1243–1251 (2017).
35. Y. Liu, D. Li, Z. Yin, X. Luo, W. Liu, W. Zhang, Z. Zhang, Y. Cao, Y. Liu, G. Zhou, Prolonged *in vitro* precultivation alleviates post-implantation inflammation and promotes stable subcutaneous cartilage formation in a goat model. *Biomed. Mater.* **12**, 015006 (2017).

36. J. Xue, A. He, Y. Zhu, Y. Liu, D. Li, Z. Yin, W. Zhang, W. Liu, Y. Cao, G. Zhou, Repair of articular cartilage defects with acellular cartilage sheets in a swine model. *Biomed. Mater.* **13**, 025016 (2018).
37. A. He, A. Ye, N. Song, N. Liu, G. Zhou, Y. Liu, X. Ye, Phenotypic redifferentiation of dedifferentiated microtia chondrocytes through a three-dimensional chondrogenic culture system. *Am. J. Transl. Res.* **12**, 2903–2915 (2020).
38. S. E. Domayer, G. H. Welsch, R. Dorotka, T. C. Mamisch, S. Marlovits, P. Szomolanyi, S. Trattnig, MRI monitoring of cartilage repair in the knee: A review. *Semin. Musculoskelet. Radiol.* **12**, 302–317 (2008).
39. W.-J. Li, H. Chiang, T.-F. Kuo, H. Lee, C.-C. Jiang, R. S. Tuan, Evaluation of articular cartilage repair using biodegradable nanofibrous scaffolds in a swine model: A pilot study. *J. Tissue Eng. Regen. Med.* **3**, 1–10 (2009).
40. H. Yuk, T. Zhang, S. Lin, G. A. Parada, X. Zhao, Tough bonding of hydrogels to diverse non-porous surfaces. *Nat. Mater.* **15**, 190–196 (2016).
41. D. Wirthl, R. Pichler, M. Drack, G. Kettlguber, R. Moser, R. Gerstmayr, F. Hartmann, E. Bradt, R. Kaltseis, C. M. Siket, S. E. Schausberger, S. Hild, S. Bauer, M. Kaltenbrunner, Instant tough bonding of hydrogels for soft machines and electronics. *Sci. Adv.* **3**, e1700053 (2017).
42. W. Yan, X. Xu, Q. Xu, Z. Sun, Q. Jiang, D. Shi, Platelet-rich plasma combined with injectable hyaluronic acid hydrogel for porcine cartilage regeneration: A 6-month follow-up. *Regen. Biomater.* **7**, 77–90 (2020).
43. C. D. Hoemann, M. Hurtig, E. Rossamacha, J. Sun, A. Chevrier, M. S. Shive, M. D. Buschmann, Chitosan-glycerol phosphate/blood implants improve hyaline cartilage repair in ovine microfracture defects. *J. Bone Joint Surg. Am.* **87**, 2671–2686 (2005).
44. A. M. Meppelink, X. Zhao, D. J. Griffin, R. Erali, T. J. Gill, L. J. Bonassar, R. W. Redmond, M. A. Randolph, Hyaline articular matrix formed by dynamic self-regenerating cartilage and hydrogels. *Tissue Eng. Part A* **22**, 962–970 (2016).
45. G. Zhou, W. Liu, L. Cui, X. Wang, T. Liu, Y. Cao, Repair of porcine articular osteochondral defects in non-weightbearing areas with autologous bone marrow stromal cells. *Tissue Eng.* **12**, 3209–3221 (2006).
46. S. K. Seidlits, Z. Z. Khaing, R. R. Petersen, J. D. Nickels, J. E. Vanscoy, J. B. Shear, C. E. Schmidt, The effects of hyaluronic acid hydrogels with tunable mechanical properties on neural progenitor cell differentiation. *Biomaterials* **31**, 3930–3940 (2010).
47. Z. Yang, Y. Shi, X. Wei, J. He, S. Yang, G. Dickson, J. Tang, J. Xiang, C. Song, G. Li, Fabrication and repair of cartilage defects with a novel acellular cartilage matrix scaffold. *Tissue Eng. Part C Methods* **16**, 865–876 (2010).

Acknowledgments: We acknowledge the technical help of Y. Xu, P. Zhang, and Z. Ci from the Guangdong Zhou's group. We also acknowledge the arthroscopic support of J. Jiang, J. Cai, and L. Wang from J. Zhao's group. **Funding:** This work was financially supported by National Key Research and Development Program of China (2019YFA0110500 and 2017YFC1103900), the National Nature Science Foundation of China (22022506 and 21774030), Shanghai Municipal Science and Technology Major Project (grant no.2018SHZDZX03), the Program of Shanghai Technology Research Leader (18XD1421500), and the China Postdoctoral Science Foundation (2020M681332). **Author contributions:** Q.L. and G.Z. provided the ideas. Y.H., G.Z., L.Z., and Q.L. were responsible for the experimental concept, design, and data analysis and wrote the manuscript. Y.H. and Y.Z. prepared materials, performed the physicochemical studies, and analyzed data. Y.H., L.J., and D.Z. performed cytotoxicity evaluation experiments and analyzed data. L.J., H.X., and S.T. performed the subcutaneous implantation experiments and analyzed data. Y.H., L.J., H.X., G.Z., and Q.L. performed animal experiments and analyzed data. J.Z., X.Y., and G.Z. performed arthroscopic surgery. G.Z., L.Z., and Q.L. provided financial support. Q.L. supervised all aspects of this work and wrote the manuscript. Y.H., H.X., and L.J. contributed equally to this work. All authors commented on the manuscript and its revisions. **Competing interests:** The authors declare that they have no competing interests. **Data and materials availability:** All data needed to evaluate the conclusions in the paper are present in the paper and/or the Supplementary Materials.

Submitted 14 December 2020
Accepted 6 July 2021
Published 25 August 2021
10.1126/sciadv.abg0628

Citation: Y. Hua, H. Xia, L. Jia, J. Zhao, D. Zhao, X. Yan, Y. Zhang, S. Tang, G. Zhou, L. Zhu, Q. Lin, Ultrafast, tough, and adhesive hydrogel based on hybrid photocrosslinking for articular cartilage repair in water-filled arthroscopy. *Sci. Adv.* **7**, eabg0628 (2021).

Science Advances

Ultrafast, tough, and adhesive hydrogel based on hybrid photocrosslinking for articular cartilage repair in water-filled arthroscopy

Yujie Hua, Huitang Xia, Litao Jia, Jinzhong Zhao, Dandan Zhao, Xiaoyu Yan, Yiqing Zhang, Shengjian Tang, Guangdong Zhou, Linyong Zhu and Qiuning Lin

Sci Adv **7** (35), eabg0628.
DOI: 10.1126/sciadv.abg0628

Science Advances (ISSN 2375-2548) is published by the American Association for the Advancement of Science, 1200 New York Avenue NW, Washington, DC 20005. The title *Science Advances* is a registered trademark of AAAS.